J Mol Model (2013) 19:1379–1389
DOI 10.1007/s00894-012-1688-5

ORIGINAL PAPER

Dynamics of DNA polymerase I (Klenow fragment) under external force

Ping Xie

Received: 26 June 2012 / Accepted: 12 November 2012 / Published online: 30 November 2012

Abstract During DNA synthesis, high-fidelity DNA polymerase (DNAP) translocates processively along the template by utilizing the chemical energy from nucleotide incorporation. Thus, understanding the chemomechanical coupling mechanism and the effect of external mechanical force on replication velocity are the most fundamental issues for high-fidelity DNAP. Here, based on our proposed model, we take Klenow fragment as an example to study theoretically the dynamics of high-fidelity DNAPs such as the replication velocity versus different types of external force, i.e., a stretching force on the template, a backward force on the enzyme and a forward force on the enzyme. Replication velocity as a function of the template tension with only one adjustable parameter is in good agreement with the available experimental data. The replication velocity is nearly independent of the forward force, even at very low dNTP concentration. By contrast, the backward force has a large effect on the replication velocity, especially at high dNTP concentration. A small backward force can increase the replication velocity and an optimal backward force exists at which the replication velocity has maximum value; with any further increase in the backward force the velocity decreases rapidly. These results can be tested easily by future experiments and are aid our understanding of the chemomechanical coupling mechanism and polymerization dynamics of high-fidelity DNAP.

Keywords DNA replication · Chemomechanical coupling · Dynamics

Introduction

High-fidelity DNA polymerase (DNAP) is able to synthesize a new DNA strand on a template strand with high efficiency as well as high specificity [1–4]. During DNA replication, high-fidelity DNAP moves processively along the template, incorporating nucleotide triphosphate (dNTP) into the 3′ end of the new strand. From a physical point of view, DNAP functions as a molecular motor, utilizing the chemical energy from nucleotide incorporation to drive the mechanical motion of the motor along the template. Thus, understanding this chemomechanical coupling mechanism and the effect of external mechanical force on the replication velocity are the most fundamental issues when studying DNAP.

Among the high-fidelity DNAPs, the Klenow fragment of *Escherichia coli* DNAP I [Pol I(KF)], an active truncated form that composed of a polymerase domain and a 3′-5′ exonuclease domain, has been studied rigorously for more than 40 years [5–7]. Structural studies have show that the polymerase domain of Pol I(KF), like those of other high-fidelity DNAPs, consists of three subdomains: the fingers, the palm, and the thumb [8–12]. Comparison of the structures of DNAP-DNA binary complexes with the corresponding DNAP-DNA-dNTP ternary complexes revealed a large movement of the fingers subdomain relative to other subdomains [13–17]. The rate of this movement of the fingers induced by nucleotide binding was measured using stopped-flow fluorescence methods [18]. Using rapid chemical quenching methods the enzyme's minimal reaction pathway was defined and the transition rates in the pathway were determined [19]. Using single-molecule optical or magnetic trapping techniques, replication velocity was also

Electronic supplementary material The online version of this article (doi:10.1007/s00894-012-1688-5) contains supplementary material, which is available to authorized users.

P. Xie (✉)
Key Laboratory of Soft Matter Physics, Institute of Physics, Chinese Academy of Sciences, Beijing 100190, China
e-mail: pxie@aphy.iphy.ac.cn

P. Xie
Beijing National Laboratory for Condensed Matter Physics, Institute of Physics, Chinese Academy of Sciences, Beijing 100190, China

studied as the enzyme catalyzes the replication of a mechanically stretched DNA template [20, 21]. To explain this observed effect of this template tension on replication velocity, several kinetic models have been proposed [20–23]. Originally, the effect of template tension on replication velocity was interpreted by making use of global force-extension curves for double stranded DNA (dsDNA) and single stranded DNA (ssDNA) [20, 21]. Later, a model was proposed that invokes only local interactions in the neighborhood of the enzyme in explaining the effect [22, 23]. In addition, the effect was also studied using molecular dynamics simulations [24, 25]. Recently, the movement of Pol I [Klenow fragment (KF)] on the template during DNA synthesis was monitored by using single-molecule fluorescence resonance energy transfer (smFRET) at single base-pair resolution [26]. Moreover, smFRET was also used to study the dynamics of strand displacement DNA synthesis by Pol I(KF) [27].

We previously proposed a model for translocation of high-fidelity DNAP along the template during processive nucleotide additions [28, 29]. In the present work, we modify the proposed model. Based on the modified model, we study theoretically and in detail the dynamics of Pol I(KF) under the effect of different types of external force during both single-stranded primer extension synthesis and strand-displacement DNA synthesis. The external forces include the template tension, which is defined as a stretching force acting on the template, the backward force acting on the enzyme, and the forward force acting on the enzyme. The results for the replication velocity as a function of the template tension are in good agreement with the available experimental data. In particular, many interesting predicted results, such as replication velocity as a function of the backward and forward forces are presented. Testing of the predicted results in future experiments will help significantly in our understanding of the chemomechanical coupling mechanism of high-fidelity Pol I(KF).

Model

In the model [28, 29], the interaction between Pol I(KF) and its DNA substrate is characterized by two DNA-binding sites located in Pol I(KF).[1] One—called binding site S_1—is composed of residues that have an affinity for the ssDNA template. Another —binding site S_2—is composed of residues that have an affinity for the upstream dsDNA. Binding site S_1 is located in the fingers subdomain (see Fig. 1a), which is supported by experimental data showing that this subdomain has a high binding affinity for the ssDNA template [30, 31]. Binding site S_2 is located in the palm and thumb subdomains (see Fig. 1a).

The interaction potentials of the two binding sites with the DNA substrate are described as follows. For convenience, we represent the position of Pol I(KF) along the DNA template by that of its polymerase active site. After incorporation of the nucleotide paired with the nth base on the template but before the binding of the next dNTP (top of Fig. 1b), the form of $V_1(x)$ is shown in Fig. 1b (middle), where E_1 is the binding affinity for all N_1 bases of the ssDNA template that the binding site S_1 can cover, and E'_1 is the binding affinity for (N_1-1) bases. Note that the binding affinity E'_1 corresponding to binding (N_1-1) bases is smaller than E_1 corresponding to binding all N_1 bases. Moreover, since, due to the structural restriction, the primer 3′ terminus is not allowed to move forward relative to Pol I (KF) when its active site is located at the primer 3′ terminus, we assume the presence of a large energy barrier on the right-hand side of $V_1(x)$ when Pol I(KF) is positioned at the nth site. Similarly, the potential, $V_2(x)$, of binding site S_2 interacting with dsDNA is shown in Fig. 1b (bottom), where E_2 denotes the binding affinity for the dsDNA containing all N_2 base pairs that the binding site S_2 can cover, and E'_2 the affinity for the dsDNA containing only (N_2-1) base pairs. As noted, the interaction between the binding site S_2 and the dsDNA is mainly via electrostatic force. On the other hand, the interaction distance of the electrostatic force is approximately equal to the Debye length (~1 nm) in solution, which is larger than the distance (p=0.34 nm) between two successive base pairs. Thus, it is expected that the height of the potential barrier in $V_2(x)$ would increase as the binding site S_2 deviates away from the dsDNA segment along the x direction (bottom of Fig. 1b). From Fig. 1b, the deepest well of the total potential, $V(x) = V_1(x) + V_2(x)$, of Pol I(KF) interacting with the DNA substrate is seen to be located at the position of the $(n+1)$th template base. Thus, Pol I(KF) is located at the position of the $(n+1)$th base almost all the time.

Another important characteristic of high-fidelity DNAPs is the rotation of the fingers subdomain from open (closed) to closed (open) conformation induced by the binding (release) of dNTP (pyrophosphate, PPi) [13–17]. It is argued that the closed conformation of the fingers activates phosphodiester bond formation (or nucleotide incorporation), while the open conformation of the fingers opens the active site for nucleotide binding.

Based on the two interaction potentials (Fig. 1b) and the characteristics of fingers rotation, as mentioned above, the translocation model of Pol I(KF) along the template during one chemomechanical coupling cycle is shown schematically in the right panels of Fig. 1. After the nucleotide complementary to the nth template base has just been incorporated,

[1] It is noted that in the translocation models for DNAPs of other families such as families X and Y [38, 39], the interaction between the enzymes and their DNA substrates can also be well characterized by distinct DNA-binding sites located in the enzymes.

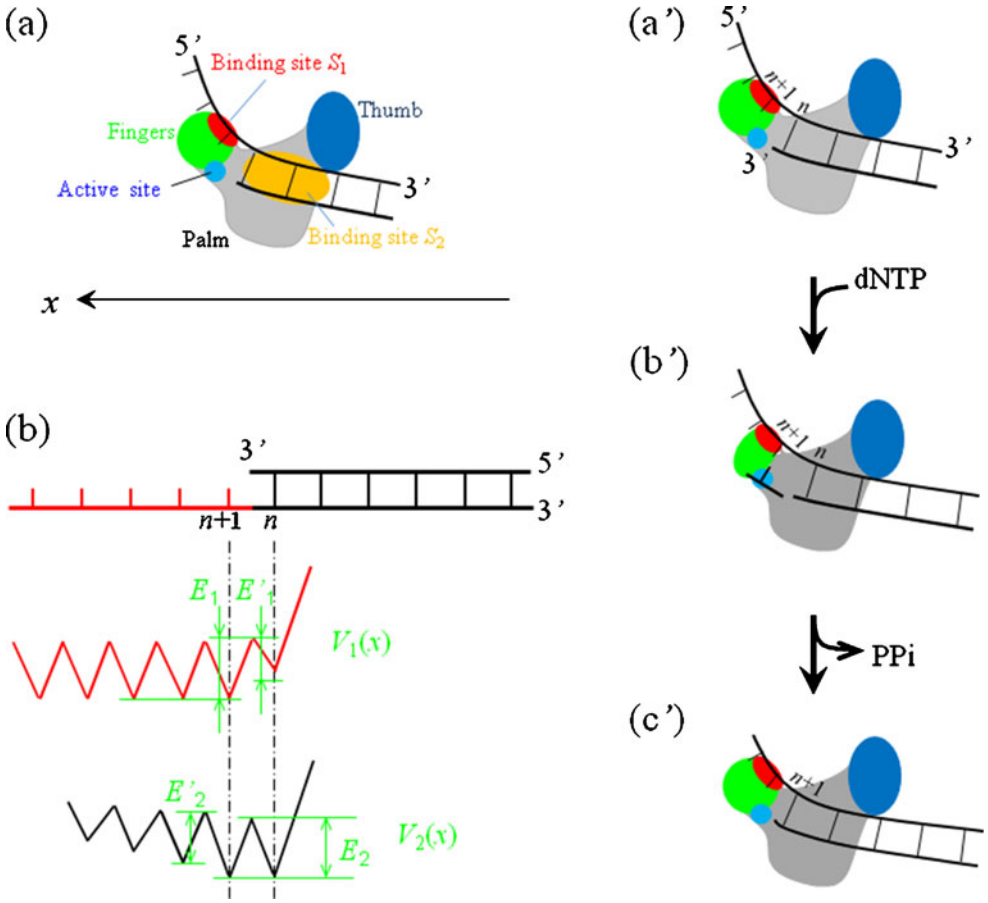

Fig. 1 Illustrations of the interaction of high-fidelity DNA polymerase (DNAP) with DNA substrate and the translocation model of DNAP along the template. **a** Schematic diagram of DNAP complexed with the DNA substrate. **b** Potentials of DNAP interacting with the DNA substrate; *top* DNA substrate after the incorporation of nucleotide paired with the *n*th base on the template but before the binding of the next dNTP, *middle* potential $V_1(x)$ of binding sites S_1 interacting with the ssDNA segment, *bottom* potential $V_2(x)$ of binding sites S_2 interacting with the dsDNA segment. *Right panels* (**a'**–**c'**) illustrate the translocation model of DNAP along the template (see text for detailed description). The *green circles* in **a'** and **c'** denote open fingers while the *green ellipse* in **b'** denote closed fingers

Pol I(KF) would move rapidly to the $(n+1)$th site due to thermal noise (see Supplementary Material), where the total interaction potential $V(x)$ between the enzyme and the DNA substrate has the deepest well (Fig. 1a').[2] Since the active site is unoccupied, the dNTP can bind to the active site at the $(n+1)$th site. The binding of dNTP sterically prevents Pol I (KF) from moving backward to the *n*th site, and induces the fingers to rotate from open to closed conformation (Fig. 1b'). The closed conformation activates nucleotide incorporation. After incorporation, the release of PPi induces the fingers to return to the open conformation. Then, driven by thermal noise, Pol I(KF) moves rapidly to the new deepest potential well (Fig. 1c'), from where the next nucleotide-incorporation cycle proceeds. In the model, the translocation step occurs after PPi release, which is supported by comparison of the available binary (Pol I(KF)-DNA) and ternary (Pol I(KF)-DNA-dNTP) structures (see, e.g., [15]).

[2] Note that, before binding of dNTP, Pol I(KF) could occasionally move backward to the *n*th site, especially if high backward external force is acting on the enzyme, where the active site is occupied by the nascent primer 3′ end, thus preventing dNTP from binding to the active site.

Reaction pathway

By using rapid chemical quenching methods Dahlberg and Benkovic [19] first defined the minimal reaction pathway for Pol I(KF) as shown in Scheme 1,where D_n and D_{n+1} represents DNA with *n* and $(n+1)$ base pairs, respectively, $E_O \cdot D_n$ and $E_O \cdot D_{n+1}$ represent binary complexes with open fingers, $E_O \cdot D_n \cdot$dNTP and $E_O \cdot D_{n+1} \cdot$PPi represent unactivated ternary complexes with open fingers, $E_C^* \cdot D_n \cdot dNTP$ and $E_C^* \cdot D_{n+1} \cdot PPi$ represent activated ternary complexes with closed fingers. The transition $E_O \cdot D_n \cdot dNTP \rightarrow E_C^* \cdot D_n \cdot dNTP$ corresponds to the rotation of fingers from open to closed conformation, while the transition $E_C^* \cdot D_{n+1} \cdot PPi \rightarrow E_O \cdot D_{n+1} \cdot PPi$ corresponds to the rotation from closed to open conformation. In our model (Fig. 1) the transition from Fig. 1a' to b' corresponds to $E_O \cdot D_n \rightarrow E_O \cdot D_n \cdot dNTP \rightarrow E_C^* \cdot D_n \cdot dNTP$ in Scheme 1, in Fig. 1b' $E_C^* \cdot D_n \cdot dNTP \leftrightarrow E_C^* \cdot D_{n+1} \cdot PPi$ occurs, and the transition from Fig. 1b' to c' corresponds to $E_C^* \cdot D_{n+1} \cdot PPi \rightarrow E_O \cdot D_{n+1} \cdot PPi \rightarrow E_O \cdot D_{n+1}$. The translocation step occurs immediately after PPi release. Since before the translocation the occupation of the active site by the primer 3′ terminus prevents the binding of dNTP, thus binding of dNTP can occur only after

$$E_O \cdot D_n \leftrightarrow E_O \cdot D_n \cdot dNTP \leftrightarrow E_C^* \cdot D_n \cdot dNTP \leftrightarrow E_C^* \cdot D_{n+1} \cdot PPi \leftrightarrow E_O \cdot D_{n+1} \cdot PPi \leftrightarrow E_O \cdot D_{n+1},$$

Scheme 1 Minimal reaction pathway for Pol I(KF)

translocation, the translocation step has an effect only on the $E_O \cdot D_n \leftrightarrow E_O \cdot D_n \cdot dNTP$ transition, while having no effect on other transitions.

Recently, using a stopped-flow fluorescence study of ternary complex formation, Joyce et al. [18] modified the minimal reaction pathway as shown in Scheme 2where, besides the states in Scheme 1, there also exists another state, $E_O^* \cdot D_n \cdot dNTP$, representing activated ternary complex with open fingers. The transition $E_O^* \cdot D_n \cdot dNTP \rightarrow E_C^* \cdot D_n \cdot dNTP$ corresponds to the rotation of fingers from open to closed conformation, while the transition $E_C^* \cdot D_{n+1} \cdot PPi \rightarrow E_O \cdot D_{n+1} \cdot PPi$ corresponds to the rotation from closed to open conformation. In our model (Fig. 1) the transition from Fig. 1a' to b' now corresponds to $E_O \cdot D_n \rightarrow E_O \cdot D_n \cdot dNTP \rightarrow E_O^* \cdot D_n \cdot dNTP \rightarrow E_C^* \cdot D_n \cdot dNTP$. In Scheme 2, k_i (i=1, 2, 3, 4, 5 and 6) denotes the forward transition rate and the corresponding backward transition rate is denoted by k_{-i}. Since the backward transition rates k_{-2}, k_{-3}, k_{-4} and k_{-6} are much smaller than their corresponding forward transition rates [19], for simplicity of analysis, we do not consider the corresponding backward transitions in Scheme 2. Then, from Scheme 2, the replication velocity k is calculated by

$$\frac{1}{k} = \frac{k_b[\mathrm{dNTP}] + k_{-1} + k_2}{k_b[\mathrm{dNTP}]k_2} + \frac{1}{k_3} + \frac{1}{k_4} + \frac{k_5 + k_{-5} + k_6}{k_5 k_6} \quad (1)$$

where k_b is the dNTP-binding rate, with $k_1 = k_b[\mathrm{dNTP}]$.

Replication velocity under template tension

To study the effect of template tension on replication dynamics, we consider a stretching force, F_T, acting on the DNA template, as performed experimentally by Maier et al. [20] and Wuite et al. [21]. From our model (Fig. 1) we note that Pol I(KF) can experience this template tension only during fingers closing and opening. Thus, from Scheme 2, the template tension F_T affects only $E_O^* \cdot D_n \cdot dNTP \leftrightarrow E_C^* \cdot D_n \cdot dNTP$ and $E_C^* \cdot D_{n+1} \cdot PPi \leftrightarrow E_O \cdot D_{n+1} \cdot PPi$ transitions, while having no effect on other transitions. Since F_T resists the transition from open to closed fingers while facilitating the transition from closed to open fingers, according to Arrhenius-Eyring kinetics, the effect of template tension F_T on transition rates k_3 and k_5 can be written as follows

$$k_3(F) = k_{30} \exp\left(-\frac{F_T d}{k_B T}\right), \quad (2a)$$

$$k_5(F) = k_{50} \exp\left(\frac{F_T d}{k_B T}\right), \quad (2b)$$

where d is the movement distance of the downstream ssDNA driven by the inward (outward) rotation of the fingers, and k_{30} and k_{50} are the transition rates under F_T=0. Since k_4 and k_6 are much larger than other rates, from Eq. (1), the replication velocity $k_c(F_T)$ at saturating dNTP concentration can be calculated approximately by

$$\frac{1}{k_c(F_T)} = \frac{1}{k_2} + \frac{1}{k_3(F_T)} + \frac{1}{k_5(F_T)}. \quad (3)$$

Since, from Eq. (1), $k_{-1} \ll k_2$, the replication velocity at any dNTP concentration has approximately the following Michaelis-Menten form

$$k(F_T) = \frac{k_c(F_T)[\mathrm{dNTP}]}{k_c(F_T)/k_b(0) + [\mathrm{dNTP}]}, \quad (4)$$

where dNTP-binding rate $k_b(0)$ is independent of F_T because F_T has no effect on the translocation of the enzyme along the template.

We first determined values of $k_b(0)$, k_2, and k_{30} from the available experimental data by using the stopped-flow fluorescence study of ternary complex formation [18]. By fitting to the experimental data for the rate of ternary complex formation versus dNTP concentration with Michaelis-Menten equation, we determined $k_b(0)$=14 $\mu M^{-1} s^{-1}$ for one template and $k_b(0)$=12 $\mu M^{-1} s^{-1}$ for another template (see Supplementary Material). Thus, we take $k_b(0)$= 13 $\mu M^{-1} s^{-1}$ in the calculation. The stopped-flow fluorescence study also determined that the rate of transition

$$E_O \cdot D_n \xleftrightarrow{k_1} E_O \cdot D_n \cdot dNTP \xleftrightarrow{k_2} E_O^* \cdot D_n \cdot dNTP \xleftrightarrow{k_3} E_C^* \cdot D_n \cdot dNTP \xleftrightarrow{k_4} E_C^* \cdot D_{n+1} \cdot PPi \xleftrightarrow{k_5} E_O \cdot D_{n+1} \cdot PPi \xleftrightarrow{k_6} E_O \cdot D_{n+1},$$

Scheme 2 Modified minimal reaction pathway

$E_O \cdot D_n \cdot dNTP \xrightarrow{k_2} E_O^* \cdot D_n \cdot dNTP$ is about 200 s^{-1} [18]. Thus, we take rate k_2=200 s^{-1}. The stopped-flow fluorescence study also indicated that, at saturating dNTP concentration, the rate of ternary complex formation is about 100 s^{-1} [18], implying that the rate of transitions $E_O \cdot D_n \cdot dNTP \xrightarrow{k_2} E_O^* \cdot D_n \cdot dNTP \xrightarrow{k_{30}} E_C^* \cdot D_n \cdot dNTP$ is about 100 s^{-1}. Thus, with this rate of 100 s^{-1} and k_2=200 s^{-1} we obtain k_{30}=200 s^{-1}. Using rapid chemical quenching methods, Dahlberg and Benkovic [19] obtained a rate of transition $E_C^* \cdot D_{n+1} \cdot PPi \rightarrow E_O \cdot D_{n+1} \cdot PPi$ of about 15 s^{-1}. Thus, we take k_{50}= 15 s^{-1}. The above rate values are summarized in Table 1. As will be seen below, the replication velocity at saturating dNTP concentration under no external force, as calculated from the transition rates given in Table 1, is consistent with different, independent experimental data. In addition, it is noted that the rate of about 100 s^{-1} for transitions $E_O \cdot D_n \cdot dNTP \rightarrow E_O^* \cdot D_n \cdot dNTP \rightarrow E_C^* \cdot D_n \cdot dNTP$, as determined in Scheme 2 [18], is close to the rate of about 50 s^{-1} determined in Scheme 1 [19].

Using Eqs. (2a), (2b) and (3) and with the parameter values given in Table 1, the calculated results of replication velocity $k_c(F_T)$ as a function of the template tension at saturating dNTP concentration are shown in Fig. 2a (line), where the only adjustable parameter d=1.6 nm. The calculated results are in good agreement with the experimental data of Maier et al. [20] (open diamonds). Moreover, it is noted that the parameter choices are robust, giving a good fit of the model to the experimental data (see Supplementary Material). To give some predicted results that can be tested easily by future in vitro experiments, we calculated the replication velocity $k(F_T)$ versus template tension at different dNTP concentrations using Eqs. (2a), (2b) and (4), with the transition rate values given in Table 1 and d=1.6 nm. Some typical results are shown in Fig. 2b. It can be seen that, as dNTP concentration decreases, the ratio of the maximum velocity at optimal tension to the velocity at no tension also decreases.

As seen from Fig. 2a, under large template tension (≥15 pN) the theoretical data are smaller than the corresponding experimental data. This is the limitation of the present model and an improved model is required, which will be done in the future.

Table 1 Parameter values used in calculations

$k_b(0)$ ($\mu M^{-1} s^{-1}$)	k_2 (s^{-1})	k_{30} (200 s^{-1})	k_{50} (s^{-1})
13[a]	200[a]	200[a]	15[b]

[a] Values determined from the available experimental data of Joyce et al. [18] using the stopped-flow fluorescence study of ternary complex formation

[b] Values determined from the available experimental data of Dahlberg and Benkovic [19] using rapid chemical quenching methods

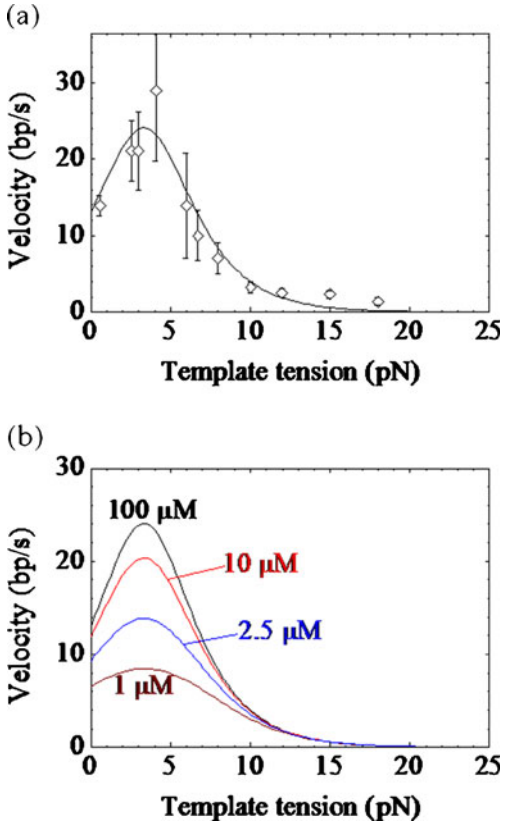

Fig. 2 Replication velocity versus template tension. **a** Results at saturating dNTP concentration: *line* calculated results, *open diamonds* experimental data measured in low stringency primer hybridization by Maier et al. [20]. **b** Calculated results at different dNTP concentrations

Replication velocity under backward external force

Consider the backward external force acting on Pol I(KF). This can be realized easily by using an optical single-trap assay in which the active molecule of Pol I(KF) is fixed to a solid surface and the end of downstream ssDNA is attached to a bead held in the trap, similar to that used by Thomen et al. [32] to measure transcription rate by RNA polymerases, or by using a dual-trap assay in which the active enzyme is attached to a bead held in a weak trap and the end of downstream ssDNA is attached to a bead held in a strong trap, similar to that used by Abbondanzieri et al. [33]. Under these experimental conditions, we have the template tension $F_T = F$.

Under the backward external force, F, which is defined as positive when it points backwards, the translocation of Pol I (KF) relative to the DNA template along the x direction in solution can be described by the following Langevin equation

$$\Gamma \frac{dx}{dt} = -\frac{\partial[V_1(x) + V_2(x)]}{\partial x} - F + \xi(t), \quad (5)$$

where x represents the position of Pol I(KF) along the template, Γ is the frictional drag coefficient on Pol I(KF), and $\xi(t)$

represents the fluctuating Langevin force with $\langle \xi(t) \rangle = 0$ and $\langle \xi(t)\xi(t') \rangle = 2k_B T\delta(t-t')$. Potentials $V_1(x)$ and $V_2(x)$ are shown in Fig. 1b. Since the jumping of Pol I(KF) from the $(n+1)$th to the $(n+2)$th site requires overcoming a larger energy barrier for $V_2(x)$ than the backward jumping to the nth site (see bottom, Fig. 1b), there would be a much smaller probability for Pol I(KF) to jump to the $(n+2)$th site than to jump to the nth site when the enzyme is positioned at the $(n+1)$th site (see Supplementary Material). Thus, for simplicity of analysis, the very small probability of jumping to the $(n+2)$th site can be negligible. Then, from Eq. (5), the mean time for Pol I(KF) to jump from the nth to the $(n+1)$th site is derived as [34, 35]

$$T_{n\to(n+1)} = \frac{l^2\Gamma k_B T}{(E_n+Fl)^2}\left[\exp\left(\frac{E_n+Fl}{k_B T}\right)-1\right] - \frac{d^2\Gamma}{E_n+Fl} + \frac{d^2\Gamma k_B T}{(E_n+Fl)(E_{n+1}-Fl)} \times \left[\exp\left(\frac{E_n+Fl}{k_B T}\right) - \exp\left(\frac{E_n-E_{n+1}+2Fl}{k_B T}\right)\right]\left[1-\exp\left(-\frac{E_n+Fl}{k_B T}\right)\left(1+\frac{E_n+Fl}{E_{n+1}-Fl}\right)\right] + \frac{d^2\Gamma}{E_{n+1}-Fl}, \quad (6)$$

where $l=p/2$, and $E_n = E_1^{'} + E_2$ and $E_{n+1} = E_1 + E_2$ are the well depths of the total potential $[V_1(x) + V_2(x)]$ at the nth and the $(n+1)$th sites, respectively. The mean time, $T_{(n+1)\to n}$, for Pol I(KF) to jump from the $(n+1)$th to the nth site can also be calculated by Eq. (6) but with E_n, E_{n+1} and F being replaced by E_{n+1}, E_n and $-F$, respectively.

As noted from Eq. (6), for $E_n >> 1\,k_B T$ and $E_{n+1} >> 1\,k_B T$, the ratio of the time, T_n, for the enzyme to stay at the nth site to the time, T_{n+1}, to stay at the $(n+1)$th site approximately has the form

$$\frac{T_n}{T_{n+1}} = \frac{T_{n\to(n+1)}}{T_{(n+1)\to n}} \approx \exp\left(\frac{\Delta E}{k_B T}\right)\exp\left(\frac{Fp}{k_B T}\right), \quad (7)$$

where $\Delta E \equiv E_n - E_{n+1} = E_1^{'} - E_1$.

Since in our model (Fig. 1) dNTP can bind to the active site only after the translocation, i.e., only during the time period T_{n+1} when the active site is positioned at the $(n+1)$th site, from Eq. (7) the dNTP-binding rate, $k_b(F)$, versus the external force F has the form

$$k_b(F) = \frac{\exp\left(\frac{\Delta E}{k_B T}\right)+1}{\exp\left(\frac{\Delta E}{k_B T}\right)\exp\left(\frac{Fp}{k_B T}\right)+1} k_b(0), \quad (8)$$

where $k_b(0)$ is the dNTP-binding rate under $F=0$. Here, we consider that the Pol I(KF) residues that are fixed to the solid surface or to the bead are far away from the active site and, thus, the effect of the external force F on the polymerase activity of the active site is only via the template tension resulting from F. From Eq. (3), we have

$$\frac{1}{k_c(F)} = \frac{1}{k_2} + \frac{1}{k_3(F)} + \frac{1}{k_5(F)}. \quad (9)$$

With $k_b(F)$ and $k_c(F)$ the replication velocity under external force F has the following Michaelis-Menten form

$$k(F) = \frac{k_c(F)[dNTP]}{k_c(F)/k_b(F) + [dNTP]}. \quad (10)$$

From Eq. (8), Eq. (10) is rewritten as

$$k(F) = \frac{k_c(F)[\mathrm{dNTP}]}{[\mathrm{dNTP}] + K_m(F)\left[\exp\left(\frac{\Delta E}{k_B T}\right)\exp\left(\frac{Fp}{k_B T}\right)+1\right]\Big/\left[\exp\left(\frac{\Delta E}{k_B T}\right)+1\right]}, \quad (11)$$

where $K_m(F) = k_c(F)/k_b(0)$.

Before studying the effect of backward force on the dynamics of Pol I(KF), we first estimated the value of ΔE for Pol I(KF) from available experimental data. As mentioned before, biochemical studies showed the presence of binding site S_1 that can interact with the ssDNA template [30, 31]. Moreover, experimental data showed that the affinity of Pol I(KF) for the DNA substrate with each additional base on the ssDNA template is increased in a stepwise manner and, as the number of the bases on the ssDNA template is increased from 1 to 4, the increased affinity relative to DNA that has one fewer template base is gradually decreased [30]. This indicates that the affinity for the first unpaired base (counted from the duplex) of the ssDNA template should have the largest value, i.e., the residue on the binding site S_1 that is closest to the duplex has the largest value. Furthermore, the experimental data showed that the affinity for the DNA of the two-nucleotide template extension is about 13-fold larger than that of a one-nucleotide template extension (see Table 1 in Ref. [30]), implying that the affinity for the second base of the ssDNA template is about $2.6\,k_B T$. In addition, considering that DNA substrates with no template overhang give unstable complexes and the small value of K_d=1.3 nM for the DNA substrate of one-nucleotide template extension (see Table 1 in Ref. [30]), it is deduced that the affinity of Pol I(KF) for the first unpaired base of the ssDNA template should be larger than $2.6\,k_B T$, implying that $E = E_1^{'} - E_1 < -2.6\,k_B T$.

Using Eqs. (9) and (11), with values of transition rates given in Table 1 and d=1.6 nm (see above), the calculated results of replication velocity, $k(F)$, versus backward force

(positive F) for different values of $\Delta E \leq -3k_BT$ are shown in Fig. 3. It can be seen that the curves of the replication velocity versus the backward force for [dNTP] ≥1 μM are nearly identical for different values of $\Delta E \leq -3k_BT$. Importantly, it is interesting to see that the backward force has a significant effect on replication velocity, especially at high dNTP concentration. A small backward force can increase the replication velocity and an optimal backward force exists at which the replication velocity reaches its maximum value. With any further increase in backward force, the velocity decreases rapidly. Moreover, by comparing Fig. 2b with Fig. 3, the effect of the backward external force is mainly via the effect of the tension on the ssDNA template that results from the external force.

Replication velocity under forward external force

Consider the forward external force acting on Pol I(KF). This can be realized easily by using an optical single-trap assay in which the Pol I(KF) molecule is fixed to a solid surface and the end of the upstream dsDNA is attached to a bead held in the trap, or by using a dual-trap assay in which the active enzyme is attached to a bead held in the weak trap and the end of the upstream dsDNA is attached to a bead held in the strong trap. Note that, under these experimental conditions, the external force has no effect on the rotation of fingers and, thus, the replication velocity at saturating dNTP concentration is calculated by

$$\frac{1}{k_c} = \frac{1}{k_2} + \frac{1}{k_3} + \frac{1}{k_5}, \tag{12}$$

where k_2, k_3 and k_5 are independent of F. The replication velocity at any dNTP concentration is still calculated by Eq. (11), where $K_m(F)$ is replaced by $K_m(0)=k_c/k_b(0)$ and F has the negative value.

Using Eqs. (11) and (12), with values of transition rates given in Table 1, the calculated results of replication velocity, $k(F)$, versus forward force (negative F) for different dNTP concentrations and different values of $\Delta E \leq -3k_BT$ are shown in Fig. 3. As in the case of backward force, different values of $\Delta E \leq -3k_BT$ also have little effect on the replication velocity for [dNTP]≥1 μM. Interestingly, the replication velocity is nearly independent of the forward external force, especially at high dNTP concentration, which is sharply distinct from the case of backward external force. Thus, we conclude that the backward and forward forces show very different features on their effects on the dynamics of Pol I(KF).

Dynamics of strand displacement DNA replication under external force

Besides the single-stranded primer extension synthesis, the dynamics of which is studied above, Pol I(KF) is also able to perform strand-displacement DNA synthesis. With near single base resolution, Schwartz and Quake [27] found that strand-displacement replication is in fact fast but is interrupted by pauses at specific DNA sequences. The experimental data of pausing dynamics [27] was well explained quantitatively by assuming the presence of an affinity of the fingers subdomain for the specific sequence of dsDNA downstream of the single strand [36].

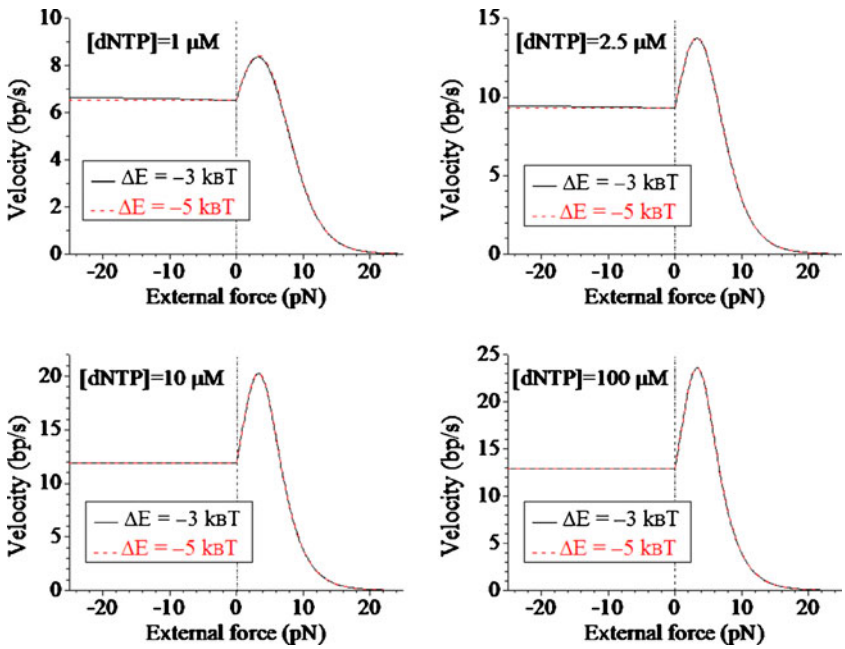

Fig. 3 Calculated results of replication velocity versus external force at different dNTP concentrations

Strand displacement replication velocity free of pauses

In the nonspecific sequence, the interaction between Pol I (KF) and DNA substrate is still considered to occur via the two binding sites S_1 and S_2, as shown in Fig. 1. Thus, the translocation of Pol I(KF) relative to the DNA template is still described by Langevin Eq. (5). However, in the equation, F is replaced by $F + F_{bp}$, where F is the external force, as defined above for single-stranded DNA synthesis, and F_{bp} is the force resulting from unwinding of a downstream base pair as Pol I(KF) translocates from the nth to the $(n+1)$th site, which is calculated approximately by $F_{bp} = E_{bp}/p$, where E_{bp} is the free energy change required to unwind one base pair [36]. Using parameters for the nearest-neighboring thermodynamic model for DNA–DNA duplex stability [37], it is estimated that the mean free energy change is about $E_{bp}=3k_BT$.

When external force F is positive (backward), $k_c(F)$ is still calculated by Eq. (9). The replication velocity free of pauses is as follows

$$k(F) = \frac{k_c(F)[\mathrm{dNTP}]}{[\mathrm{dNTP}] + K_m(F)\left[\exp\left(\frac{\Delta E}{k_BT}\right)\exp\left(\frac{(F+F_{bp})p}{k_BT}\right)+1\right]\Big/\left[\exp\left(\frac{\Delta E}{k_BT}\right)+1\right]}, \quad (13)$$

where $K_m(F) = k_c(F)/k_b(0)$ and $k_c^{-1}(F) = k_2^{-1} + k_3^{-1}(F) + k_5^{-1}(F)$ is dependent of the external force F.

When F is negative (forward), k_c is still calculated by Eq. (12). The replication velocity free of pauses is still calculated by Eq. (13), where $K_m(F)$ is replaced by $K_m(0)=k_c/k_b(0)$ and $k_c^{-1} = k_2^{-1} + k_3^{-1} + k_5^{-1}$ is independent of F.

Using Eq. (13), with values of transition rates given in Table 1 and d=1.6 nm (see above), the calculated results of strand displacement replication velocity, $k(F)$, free of pauses versus external force (both forward and negative F) for different dNTP concentrations and reasonable values of ΔE ($-6k_BT \le \Delta E \le -4k_BT$) are shown in Fig. 4 (solid lines, curves 1, 2 and 3), where, for comparison, we also show the corresponding results of single-stranded DNA replication velocity versus F (dashed lines, curves 4). First, it is seen that, at saturating dNTP concentration (100 μM), the curve of strand displacement replication velocity versus external force is nearly coincident with that for single-stranded replication, although the two have substantial differences in their energetics, which is in agreement with the single-molecule experimental data of Schwartz and Quake under no external force [27]. Moreover, the replication velocity of about 13 bp/s under no external force is also consistent with the experimental data (about 14 bp/s) of Schwartz and Quake [27]. Second, as dNTP concentration decreases, deviation between velocity of strand displacement replication and that of single stranded replication. increases The deviation is more evident near the optimal backward force at which the replication velocity reaches the maximum value.

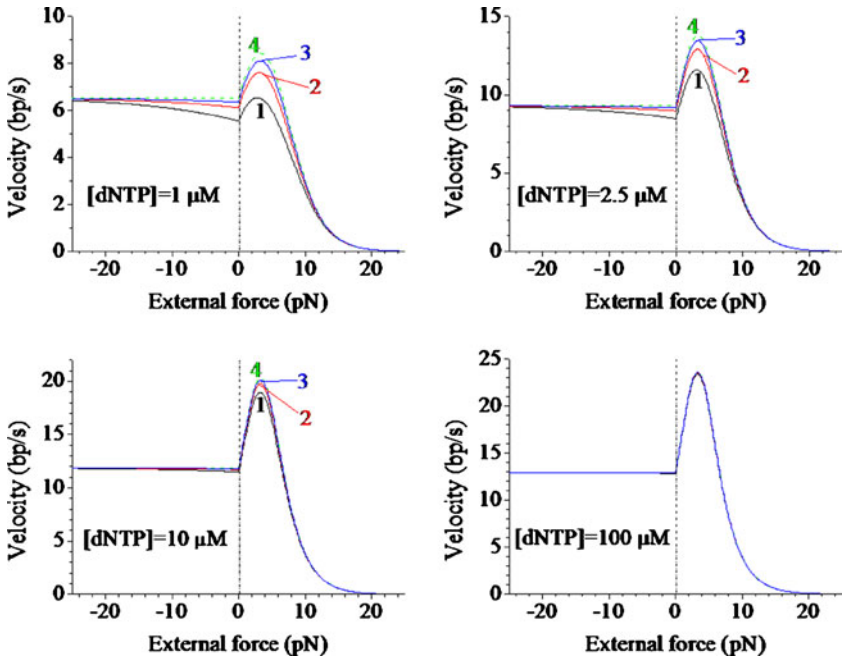

Fig. 4 Calculated results of strand displacement replication velocity free of pauses versus external force at different dNTP concentrations and for different values of ΔE. $\Delta E=-4k_BT$ (curve 1), $-5k_BT$ (curve 2) and $-4k_BT$ (curve 3). Curve 4 represents the corresponding single-stranded DNA replication velocity for $\Delta E=-5k_BT$. At [dNTP]=100 μM, the four curves 1, 2, 3 and 4 are nearly coincident

Sequence-dependent pauses

At specific sequences of dsDNA downstream of the active site, besides the presence of the interactions with potentials $V_1(x)$ and $V_2(x)$ between Pol I(KF) and the DNA substrate, another interaction between the fingers and dsDNA is assumed to be present [36]. This site-specific interaction potential $V_3(x)$ is shown in Fig. 5a, with E_3 being the binding affinity. Since the site-specific interaction is considered to be driven mainly by short-range hydrogen bonding, we take the interaction distance to be equal to p. The movement of Pol I(KF) along the template is still described by Langevin

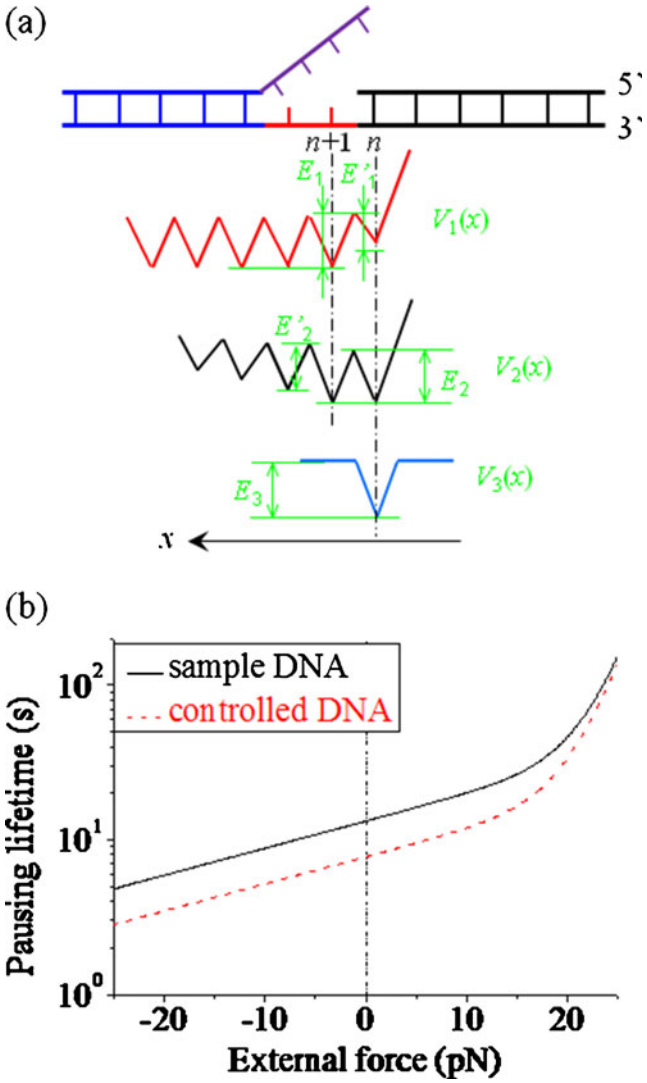

Fig. 5 Illustrations of the interaction of DNAP with DNA substrate and results for mean pausing lifetime at specific sequences of dsDNA during strand displacement replication. **a** Potentials $V_1(x)$, $V_2(x)$ and $V_3(x)$ of DNAP interacting with the DNA substrate: *top* DNA substrate after incorporation of nucleotide paired with the nth base on the template but before binding of the next dNTP. **b** Calculated results of mean pausing lifetime versus the external force F at specific sequences of dsDNA at saturating dNTP concentration

Eq. (5) but with $V_1(x) + V_2(x)$ being replaced by $V_1(x) + V_2(x) + V_3(x)$. Thus, the mean time, $T_{n\to(n+1)}$, for Pol I(KF) to jump from the nth site of specific sequence to the $(n+1)$th site is still calculated by Eq. (6) but with $E_n = E_1' + E_2 + E_3$, $E_{n+1} = E_1 + E_2$ and F is replaced by $F + F_{bp}$.

Under no external force, the experimental data for sequence-dependent pauses [27] have been explained quantitatively by considering the addition of potential $V_3(x)$ in a previous work [36]. Here, we study the effect of external force F on the pausing lifetime. At saturating dNTP concentration, the pausing lifetime is calculated by

$$T_{pause} = 1/k_c + T_{n\to(n+1)}, \tag{14}$$

where k_c is still calculated by Eq. (9) when F is positive (backward) and k_c is calculated by Eq. (12) when F is negative (forward).

Here, we study the pausing lifetimes at the specific sequence of the sample DNA substrate and that of the controlled DNA substrate, as used in Schwartz and Quake [27], where it was shown experimentally that, under no external force and at 23 °C, the pausing lifetime T_{pause}=13.2 s at the specific sequence of the former substrate and T_{pause}=7.7 s at that of the latter substrate.

Using Eqs. (6) and (14), it is calculated that T_{pause}=13.2 s corresponds to the affinity $E_1' + E_2 + E_3 = 28.18 k_B T$ and T_{pause}=7.7 s to $E_1' + E_2 + E_3 = 27.62 k_B T$ under F=0. The calculated results of the pausing lifetime versus the external force F at the specific sequence of the two DNA substrates are shown in Fig. 5b. The pausing lifetime is seen to decrease exponentially with the increase of the forward force and to increase exponentially with the increase in backward force when $F \leq 10$ pN, where the lifetime is determined dominantly by the jump time $T_{n\to(n+1)}$ from the nth site of the specific sequence to the next $(n+1)$th site and the effect of k_c on the lifetime is negligibly small. For $F > 12$ pN, the lifetime increases more rapidly with the increase of the backward force because, besides $T_{n\to(n+1)}$ the polymerase rate k_c also has a significant effect on the lifetime.

Concluding remarks

In this work, based on our proposed model, we studied analytically the replication velocity of Pol I(KF) under three types of external force, i.e., the stretching force on the template, the backward force on the enzyme and the forward force on the enzyme. Our studies yielded the following results. The template tension has a large effect on replication velocity, especially at high dNTP concentration and, as dNTP concentration decreases, the effect of template tension also decreases. The replication velocity is nearly independent of the forward external force even at very low dNTP

concentrations of 1 μM. By contrast, the backward external force has a large effect on replication velocity, especially at high dNTP concentration. A small backward force can increase replication velocity and an optimal backward force exists at which replication velocity has its maximum value. With any further increase in backward force, velocity decreases rapidly. All these predicted results (Figs. 2b, 3, 4) can be tested easily by future experiments. A straightforward comparison of the predicted results with the experimental data has important implications for our understanding of the working mechanism and polymerization dynamics of high-fidelity DNAPs.

Acknowledgments This work was supported by the National Natural Science Foundation of China (Grant No. 10974248).

References

1. Lodish H, Berk A, Zipursky SL, Matsudaira P, Baltimore D, Darnell J (2000) Molecular cell biology, 4th edn. Freeman, New York, Chapter 12
2. Echols H, Goodman MF (1991) Fidelity mechanisms in DNA replication. Annu Rev Biochem 60:477–511
3. Johnson KA (1993) Conformational coupling in DNA polymerase fidelity. Annu Rev Biochem 62:685–713
4. Joyce CM, Steitz TA (1994) Function and structure relationships in DNA polymerase. Annu Rev Biochem 63:777–822
5. Klenow H, Henningsen I (1970) Selective elimination of the exonuclease activity of the deoxyribonucleic acid polymerase from *Escherichia coli B by limited proteolysis. Proc Natl Acad Sci USA 65:168–175*
6. Bebenek K, Joyce CM, Fitzgerald MP, Kunkel TA (1990) The fidelity of DNA synthesis catalyzed by derivatives of *Escherichia coli* DNA polymerase I. J Biol Chem 265:13878–13887
7. Patel PH, Suzuki M, Adman E, Shinkai A, Loeb LA (2001) Prokaryotic DNA polymerase I: evolution, structure, and "base flipping" mechanism for nucleotide selection. J Mol Biol 308:823–837
8. Ollis DL, Brick P, Hamlin R, Xuong NG, Steitz TA (1985) Structure of large fragment of *Escherichia coli* DNA polymerase I complexed with dTMP. Nature 313:762–766
9. Korolev S, Nayal M, Barnes WM, Di Cera E, Waksman G (1995) Crystal structure of the large fragment of *Thermus aquaticus* DNA polymerase I at 2.5- Å resolution: structural basis for thermostability. Proc Natl Acad Sci USA 92:9264–9268
10. Kim Y, Eom SH, Wang J, Lee DS, Suh SW, Steitz TA (1995) Crystal structure of *Thermus aquaticus* DNA polymerase. Nature 376:612–616
11. Eom SH, Wang J, Steitz TA (1996) Structure of Taq polymerase with DNA at the polymerase active site. Nature 382:278–281
12. Kiefer JR, Mao C, Hansen CJ, Basehore SL, Hogrefe HH, Braman JC, Beese LS (1997) Crystal structure of a thermostable *Bacillus* DNA polymerase I large fragment at 2.1 A resolution. Structure 5:95–108
13. Doublie S, Ellenberger T (1998) The mechanism of action of T7 DNA polymerase. Curr Opin Struct Biol 8:704–712
14. Doublie S, Tabor S, Long AM, Richardson CC, Ellenberger T (1998) Crystal structure of a bacteriophage T7 DNA replication complex at 2.2 Å resolution. Nature 391:251–258
15. Li Y, Korolev S, Waksman G (1998) Crystal structures of open and closed forms of binary and ternary complexes of the large fragment of *thermus aquaticus* DNA polymerase I: structural basis for nucleotide incorporation. EMBO J 17:7514–7525
16. Doublie S, Sawaya MR, Ellenberger T (1999) An open and closed case for all polymerases. Structure 7:R31–R35
17. Huang H, Chopra R, Verdine GL, Harrison SC (1998) Structure of a covalently trapped catalytic complex of HIV-1 reverse transcriptase: implications for drug resistance. Science 282: 1669–1675
18. Joyce CM, Potapova O, DeLucia AM, Huang X, Basu VP, Grindley NDF (2008) Fingers-closing and other rapid conformational changes in DNA polymerase I (Klenow fragment) and their role in nucleotide selectivity. Biochemistry 47:6103–6116
19. Dahlberg ME, Benkovic SJ (1991) Kinetic mechanism of DNA polymerase I (Klenow fragment): identification of a second conformational change and evaluation of the internal equilibrium constant. Biochemistry 30:4835–4843
20. Maier B, Bensimon D, Croquette V (2000) Replication by a single DNA polymerase of a stretched single-stranded DNA. Proc Natl Acad Sci USA 97:12002–12007
21. Wuite GJL, Smith SB, Young M, Keller D, Bustamante C (2000) Single-molecule studies of the effect of template tension on T7 DNA polymerase activity. Nature 404:103–106
22. Goel A, Frank-Kamenetskii MD, Ellenberger T, Herschbach D (2001) Tuning DNA "strings": modulating the rate of DNA replication with mechanical tension. Proc Natl Acad Sci USA 98:8485–8489
23. Goel A, Astumian RD, Herschbach D (2003) Tuning and stretching a DNA polymerase motor with mechanical tension. Proc Natl Acad Sci USA 100:9699–9704
24. Andricioaei I, Goel A, Herschbach D, Karplus M (2004) Dependence of DNA polymerase replication rate on external forces: a model based on molecular dynamics simulations. Biophys J 87:1478–1497
25. Venkatramani R, Radhakrishnan R (2008) Computational study of the force dependence of phosphoryl transfer during DNA synthesis by a high fidelity polymerase. Phys Rev Lett 100:088102
26. Christian TD, Romano LJ, Rueda D (2009) Single-molecule measurements of synthesis by DNA polymerase with base-pair resolution. Proc Natl Acad Sci USA 106:21109–21114
27. Schwartz JJ, Quake SR (2009) Single molecule measurement of the "speed limit" of DNA polymerase. Proc Natl Acad Sci USA 106:20294–20299
28. Xie P (2007) Model for forward polymerization and switching transition between polymerase and exonuclease sites by DNA polymerase molecular motors. Arch Biochem Biophys 457:73–84
29. Xie P (2009) A possible mechanism for the dynamics of transition between polymerase and exonuclease sites in a high-fidelity DNA polymerase. J Theor Biol 259:434–439
30. Turner RM, Grindley NDF, Joyce CM (2003) Interaction of DNA polymerase I (Klenow fragment) with the single-stranded template beyond the site of synthesis. Biochemistry 42: 2373–2385
31. Datta K, Wowor AJ, Richard AJ, LiCata VJ (2006) Temperature dependence and thermodynamics of Klenow polymerase binding to primed-template DNA. Biophys J 90:1739–1751
32. Thomen P, Lopez PJ, Heslot F (2005) Unravelling the mechanism of RNA-polymerase forward motion by using mechanical force. Phys Rev Lett 94:128102
33. Abbondanzieri EA, Greenleaf WJ, Shaevitz JW, Landick R, Block SM (2005) Direct observation of base-pair stepping by RNA polymerase. Nature 438:460–465

34. Xie P (2009) Molecular motors that digest their track to rectify Brownian motion: processive movement of exonuclease enzymes. J Phys Condens Matter 21:375108
35. Xie P (2012) A dynamic model for processive transcription elongation and backtracking long pauses by multi-subunit RNA polymerases. Proteins 80:2020–2034
36. Xie P (2012) Modeling translocation dynamics of strand displacement DNA synthesis by DNA polymerase I. J Mol Model 18:1951–1960
37. SantaLucia J Jr (1998) A unified view of polymer, dumbbell, and oligonucleotide DNA nearest-neighbor thermodynamics. Proc Natl Acad Sci USA 95:1460–1465
38. Xie P (2011) A model for the dynamics of mammalian family X DNA polymerases. J Theor Biol 277:111–122
39. Xie P (2011) A nucleotide binding rectification Brownian ratchet model for translocation of Y-family DNA polymerases. Theor Biol Med Model 8:22